Carbon 231 (2025) 119695

Contents lists available at ScienceDirect

Carbon

journal homepage: www.elsevier.com/locate/carbon

Transition metal carbo chalcogenides: A novel family of 2D solid lubricants

Philipp G. Grützmacher [a,**], Ahmad Majed [b], Edoardo Marquis [c], Xudong Sui [a,d], M. Clelia Righi [c,*], Markus Sauer [e], Annette Foelske [e], Michael Naguib [b,f], Carsten Gachot [a,***]

[a] Institute of Design Engineering and Product Development, Research Unit Tribology, Technische Universität Wien, Lehárgasse 6, 1060, Vienna, Austria
[b] Department of Physics and Engineering Physics, Tulane University, New Orleans, LA, 70118, USA
[c] Department of Physics and Astronomy, Alma Mater Studiorum – University of Bologna, Viale Berti Pichat 6/2, 40127, Bologna, Italy
[d] State Key Laboratory of Solid Lubrication, Lanzhou Institute of Chemical Physics, Chinese Academy of Sciences, Lanzhou, 730000, China
[e] Analytical Instrumentation Center, Technische Universität Wien, Lehárgasse 6, 1060, Vienna, Austria
[f] Department of Chemistry, Tulane University, New Orleans, LA, 70118, USA

ARTICLE INFO

Keywords:
Friction
Wear
2D layered materials
Transition metal carbo-chalcogenides (TMCCs)
Solid lubrication

ABSTRACT

Two-dimensional (2D) layered materials such as transition metal dichalcogenides (e.g., MoS_2, WS_2) and MXenes (e.g., $Ti_3C_2T_x$), as well as hybrids of these materials are the focus of current research in solid lubrication due to their outstanding performance. Transition metal carbo-chalcogenides (TMCCs), consisting of an MXene core and a TMD-like surface, represent an inherent combination of TMDs and MXenes without the need to construct hybrids out of the individual layers. Due to their layered structure and surface chemistry, favorable tribological properties can be expected from these novel materials. Here, multilayer Ta_2S_2C and Nb_2S_2C TMCCs are deposited solely as a powder onto a steel substrate and their tribological properties under linear sliding against different counterbodies, i.e., Al_2O_3, SiC, 100Cr6, and polytetrafluoroethylene (PTFE) are discussed. Advanced materials characterization techniques are used to detect the presence of TMCCs inside the wear tracks and to reveal their 2D structure within the tribofilm. Finally, density functional theory (DFT) simulations are used to unravel the easy shearability of TMCCs at the nanoscale. The results demonstrate the great potential of this new 2D material family, which also offers many possibilities for defined tuning of the solid-solid interface.

1. Introduction

Many technological advances are only possible through the discovery of new and advanced materials. An example is the transition to clean energy, which is fueled by applied material science, making it possible to further reduce the cost of electricity from solar and wind or improve the efficiency of electric vehicles [1]. A possibility to save energy is often overlooked, which is to reduce friction and wear. However, the amount of energy wasted by friction and wear is excessive. This inspires the search for new lubricating materials, which demonstrate lower friction, protect the surfaces more from wear, and are stable over a wide range of conditions. Problems associated with the disposal of liquid lubricants and their limited thermal and chemical stability favor solid lubricating materials for example in space applications [2,3]. Two-dimensional (2D) materials with layered structures have been the focus of research as solid lubricant materials due to their exceptional mechanical, physical, and chemical properties [4–7]. These properties stem from their unique structure, where the atoms within a layer (in-plane atoms) are held together by a mixture of ionic and/or covalent bonds, providing high strength. Meanwhile, adjacent out-of-plane layers are weakly bonded, interacting mainly through van der Waals (vdW) forces. This configuration results in atomic planes with a high strength yet can easily shear over each other. Nanosheets can exhibit very low friction (i.e., superlubricity with a coefficient of friction lower than 0.01), provided adequate operation conditions [8]. Due to their advantages in terms of vacuum and temperature stability, contamination resistance, and low friction, solid lubricants such as MoS_2 or WS_2 (Dicronite [9]) are the lubricating materials of choice for many space applications (e.g., Mars Rover, James Webb Space Telescope) [10]. However, challenges remain, such as their short wear life and the dependence of their tribological performance on the environmental conditions [4]. For instance, MoS_2 produces very low friction in vacuum or inert gas but

* Corresponding author.
** Corresponding author.
*** Corresponding author.
E-mail addresses: philipp.gruetzmacher@tuwien.ac.at (P.G. Grützmacher), clelia.righi@unibo.it (M.C. Righi), carsten.gachot@tuwien.ac.at (C. Gachot).

https://doi.org/10.1016/j.carbon.2024.119695
Received 28 July 2024; Received in revised form 11 September 2024; Accepted 8 October 2024
Available online 11 October 2024

reacts with humidity and oxygen in air to form MoO_3, thereby losing its exceptional tribological performance [11]. A possibility to further improve the properties of 2D materials and to unlock synergistic effects is to stack different 2D materials into vdW heterostructures or nanocomposites [12]. Numerous examples demonstrate that the friction and wear performance of 2D heterostructures and nanocomposites is greatly improved compared to their individual components. These include graphene/transition metal dichalcogenide (TMD) heterostructures [12], TMD/TMD heterostructures, e.g., $MoS_2/MoSe_2$ [13], or $Ti_3C_2T_x/MoS_2$ nanocomposites [14,15]. Often, even superlubricity is achieved in these systems due to the intrinsic lattice mismatch between two different 2D materials, rendering the systems naturally incommensurate [13].

MXenes, which are layered transition metal carbides, nitrides, or carbonitrides first synthesized in 2011 [16], represent an extensive family of 2D materials. Their properties can be tuned by leveraging their significant structural and chemical versatility [17]. Their tunability has sparked interest in the tribological community [18,19], and experimental testing has demonstrated very interesting performance, specifically in terms of outstanding wear life compared to MoS_2 or even WS_2 [20,21]. Additionally, under the right conditions even superlubric regimes can be achieved [22,23]. Nevertheless, the issue with environmental sensitivity remains a challenge [24]. Utilizing the aforementioned heterostructures or nanocomposites might be a viable option to expand the parameter space for sustaining effective lubrication. Indeed, combinations of MXenes i.e., $Ti_3C_2T_x$ with MoS_2 [14] or $MoSe_2$ [25] have proven to provide very low friction (even in the superlubric range between 0.007 and 0.01). In recent years, considerable effort has been devoted to understanding and designing interfaces involving TMDs and MXenes.

On the other hand, the tribological community completely overlooked a family of new 2D materials, which can be considered an inherent and exciting combination of MXenes and TMDs, so called transition metal carbo-chalcogenides (TMCCs) [26]. Although the synthesis of many TMCCs in bulk 3D-form such as Ta_2S_2C and Nb_2S_2C had already been achieved in the past century [27,28], it is only thanks to the successful exfoliation of TMCCs into single layers achieved by some of the authors [26], that this family of 2D materials has definitely gained the attention of the scientific community, especially in the fields of electrochemical energy conversion and storage [29]. However, we could not find any extensive report on their usage as solid lubricants in the literature. To date, there is only one study investigating the tribological properties of Ta_2S_2C and $(Ta, Nb)_2S_2C$ transition metal carbo-chalcogenides [30]. In their 1998 work [30], Wally and Ueki reported promising tribological properties of bulk carbosulfides, but the research did not continue, and the family of 2D materials remained unexplored until today. Compared to heterostructures, TMCCs have the advantage that the solid/solid interface can be engineered in a very controlled fashion, they can be considered as an interface-free hybrid of TMD and MXene. The intriguing combination of a MXene core and a TMD surface might give important insights into the role of mechanical stability provided by the layer core, and the chemical composition of the surface determining environmental stability, reactivity, and interlayer binding, all of which affect tribological behavior.

Herein, we describe the tribological properties of multilayer Ta_2S_2C and Nb_2S_2C TMCCs deposited solely as powders onto 100Cr6 steel substrate, in linear reciprocating sliding against different counterbody materials, i.e., Al_2O_3, SiC, 100Cr6, and polytetrafluoroethylene (PTFE). Despite the simplicity of this first explorative approach, the presence of TMCC powders in the contact area is sufficient in most cases to maintain a coefficient of friction (COF) lower than 0.2, which is considered a threshold for effective solid lubrication [31,32]. The lubrication ability of TMCC is traced back to the tribo-induced formation of a compacted patchy tribofilm, which reduces the COF and prevents the substrate from wear. X-ray photoelectron spectroscopy (XPS) and Auger-Meitner electron spectroscopy (AMES) highlighted the presence of TMCCs inside the wear tracks. The 2D structure of TMCCs was detected inside the tribofilm by transmission electron microscopy (TEM). Finally, density functional theory (DFT) simulations were carried out to confirm the easy-to-shear ability of TMCCs, suggesting that their 2D structure can accommodate shear between layers.

2. Materials and methods

2.1. Synthesis and characterization of TMCCs

Niobium carbo-sulfide (Nb_2S_2C) and tantalum carbo-sulfide (Ta_2S_2C) were obtained by solid-state synthesis followed by chemical purification. $Fe_xNb_2S_2C$ was synthesized using commercial precursors of niobium (Nb, 99.8 %, <45 μm, Alfa Aesar), niobium carbide (NbC, 99 %, <10 μm, Alfa Aesar), iron (II) sulfide (FeS, 99 %, 60–200 μm, STREM). Powders with an atomic ratio of Nb: NbC: FeS = 1.0: 1.0: 1.5 were weighed inside an Argon (Ar)-filled glovebox. Yttrium stabilized zirconia balls (10 balls, 5 mm each) were added to high density polyethylene container as mixing media along with the powders. The container was sealed with parafilm in the glovebox, then transferred outside the glovebox to a Turbula T2F mixer, where it was mixed at ~56 rpm for 3 h. The mixed powders were returned to the glovebox and cold-pressed under 300 bars into 1-inch pellets. These pelletized samples were then placed in an alumina crucible inside a tube furnace and heated under a constant Ar flow at a rate of 10 °C/min to 1550 °C, where they were held for 30 min. The pellets were then allowed to cool to room temperature. After cooling, the pellets were pulverized and sieved through a 325 mesh (<44 μm). ***Nb_2S_2C*** was obtained by etching $Fe_xNb_2S_2C$ using aqueous hydrochloric acid (12 M HCl) with a ratio of 20 ml HCl for each 1 g of starting powder. The solution was heated to 30 °C using a hot plate for 48 h and mixed with the aid of a Teflon-coated magnetic stir bar. The sample was washed with deionized (DI) water until near neutral pH was reached. Similarly, $Fe_xTa_2S_2C$ was synthesized by mixing tantalum (Ta, 99.9 %, <150 μm, Alfa Aesar), tantalum carbide (TaC, 99.5 %, <44 μm, Alfa Aesar), and iron (II) sulfide in a molar ratio of Ta: TaC: FeS = 1.0: 1.0: 1.75. ***Ta_2S_2C*** was obtained from $Fe_xTa_2S_2C$ by mixing the ground sample (<44 μm) with 12 M HCl at 30 °C for 48 h followed by washing. After washing the sample with DI water to a pH ~7, the dried sample was obtained by vacuum-assisted filtration.

The crystal structures of the investigated samples were analyzed using a Rigaku D/Max-2200 X-ray diffractometer with a Cu Kα source. Scans were performed with a 2θ step size of 0.02° and a sweep rate of 1°/min. Scanning electron microscope (SEM) images were obtained using a Hitachi S-4800 microscope at an acceleration voltage of 3 kV, while images were processed with an image processing software (ImageJ). Chemical compositions were confirmed through energy dispersive x-ray spectroscopy (EDS) analysis with an Oxford-Hitachi S-3400 microscope at an accelerating voltage of 30 kV.

2.2. Tribological experiments

Frictional testing of the TMCCs was conducted using a ball-on-disk tribometer (*Rtec Instruments, MFT-2000A*) in linear reciprocating sliding with a stroke length of 1 mm. As substrate material we used AISI 304 steel platelets with a size of 20 x 20 × 1 mm^3, Young's modulus of 200 GPa, Poisson ratio of 0.29, and an initial roughness Sq of 0.18 μm. Various counterbody materials were employed (Al_2O_3, SiC, 100Cr6, and PTFE). All had a diameter of 6 mm, except for PTFE, which was 6.35 mm. The linear sliding velocity was set at 1 mm/s and the normal force was 0.25 N. This load corresponds to Hertzian contact pressure of 0.45, 0.48, 0.40 and 0.012 GPa for Al_2O_3, SiC, 100Cr6 and PTFE. The temperature during the measurements ranged between 19.5 and 24.8 °C, and the relative humidity between 23 % and 46 %. After mounting the sample in the tribometer, we deposited the synthesized TMCCs powder onto the substrate using a spatula. Although this method does not ensure strong adhesion to the substrate, it served as a useful test to evaluate the performance of the TMCCs powder without employing more advanced

deposition techniques. About 10 ± 2 mg of powder was spread over the steel substrate. Then, the counterbody was brought into contact with the TMCC powder, ensuring visible transfer of the loose powder from the substrate to the counterbody. Afterwards, the sliding tests started. Additionally, tests without powder addition were run. The tribological experiments were repeated three times for statistical representation, and the curves were used to calculate the corresponding mean values and standard deviations.

Linear reciprocating sliding tests were repeated using WS_2 and $Ti_3C_2T_x$ MXene powders as benchmark materials. We used the same tribological parameters as previously described (i.e., stroke length = 1 mm, sliding velocity = 1 mm/s, normal force = 0.25 N) with an Al_2O_3 counterbody, resulting in a Hertzian contact pressure of 0.45 GPa. Details about the benchmarking materials (WS_2 and $Ti_3C_2T_x$) are summarized in the Supporting Information, according to Ref. [33] and Ref. [34].

2.3. Surface characterization after wear

All samples were imaged by confocal laser scanning microscopy (*CLSM, Keyence VK-X1100*) before and after the friction tests.

The XPS measurements were carried out on a PHI Versa Probe III-spectrometer equipped with a monochromatic Al-Kα X-ray source and a hemispherical analyser (acceptance angle: ±20°). Pass energies of 55 eV and step widths of 0.1 eV were used for XPS detail spectra (Excitation energy: 1486.6 eV; Beam energy and spot size: 12.5 W onto 50 μm; Mean electron take-off angle: 45° to sample surface normal; Base pressure: $< 8 \times 10^{-10}$ mbar; Pressure during measurements: $< 1 \times 10^{-8}$ mbar). Samples were mounted on double-sided polymer tape. Electronic and ionic charge compensation was used for all measurements (automatized as provided by PHI). Surface cleaning was carried out using a gas cluster ion source (2.5 kV, 10 nA, 15min). Data analysis was performed using CASA XPS and Multipak software packages, employing transmission corrections, Shirley/Tougaard backgrounds [35,36], and customised Wagner sensitivity factors [37]. Deconvolution of spectra was carried out by using a Voigtian line shape (LA(50)). The assignment of specific binding energies to chemical components and/or bonding environments was primarily done using Refs. [38–40]. Two characteristic peaks were used to characterize Nb_2S_2C (in Nb $3d_{5/2}$ at 202.8 eV, assigned to S–Nb–C bonding) and Ta_2S_2C (in Ta $4f_{7/2}$ at 23.7 eV, assigned to S–Ta–C bonding), according to Majed et al. [26].

All Auger-Meitner Electron Spectroscopy (AMES) and EDS measurements were carried out on a PHI 710-spectrometer equipped with a field emission gun electron source, a cylindrical mirror analyser (AMES) and an Oxford Instruments Ultim©Max 100 detector (EDS). Excitation energy: 10 kV@10 nA used for AMES and EDS. AMES/EDS maps are recorded using 256x256 and 512x512 pixels (1024 channels, process time: 5 ms), respectively. Image stabilisation is used for AMES maps. AMES survey spectra were recorded in a range from 50 to 2200 eV in 0.5 eV steps (3 scans). The base system pressure was $<1 \times 10^{-9}$ mbar and pressure during measurements: $< 1 \times 10^{-8}$ mbar. While the samples were on the same holder also used in XPS, additional Cu/Be clamps were added for a better electrical contact of the sample surface. Data analysis was carried out using PHI Multipak (AMES) and Oxford AZTEC (EDS) software packages. The relative sensitivity factors are provided by PHI.

Transition electron microscopy (TEM, FEI TECNAI F20) was used to image the structure of the formed tribofilms. EDS inside the transmission electron microscope was performed using an EDAX-AMETEK Apollo XLTW SDD system. For TEM investigation, a thin lamella was prepared by ThermoFisher Scios II Focused Ion Beam (FIB). The TEM lamellae had a size of ~30 × 10 μm^2, with a thickness of < 100 nm at the regions of interest. Selected Area Electron Diffraction (SAED) patterns were used for phase analysis. Additional, high resolution-TEM (HR-TEM) imaging was performed for phase analysis using Fourier Transformation (FT) and the measurements of lattice spacings in the HR-TEM images.

2.4. Numerical simulations

We carried out Density Functional Theory (DFT) simulations by using the Quantum ESPRESSO software (version 7.2) [41–43]. The Perdew-Burke-Ernzerhof (PBE) exchange-correlation functional was employed [44], with the inclusion of van der Waals corrections according to Grimme's D2 method [45]. In particular, the standard C_6 coefficient and the van der Waals radius R_0 parameters of the metal atoms (Nb and Ta) have been replaced with those of the preceding noble gas in the periodic table (Kr and Xe, respectively). This scheme (referred to as $D2_{NG}$) was widely validated by some of the authors, providing a better description of the dispersion forces involving transition metal atoms with positive oxidation states inside 2D-materials [46]. The electronic wave-function (charge density) was expanded on a plane-waves basis truncated with a cutoff of 50 Ry (400 Ry), while ionic species were treated with "rrkj" ultrasoft pseudopotentials. Convergence thresholds of 10^{-4} Ry and 10^{-3} Ry/Bohr for the total energy were adopted for atomic relaxations. We adopted a Gaussian smearing of 0.02 Ry to describe the electronic states occupation around the Fermi level. Both Nb_2S_2C and Ta_2S_2C were modeled through trigonal unit cells (group symbol $R\bar{3}m$, group number 166), whose Brillouin zone was sampled with a 16x16x1 Monkhorst-Pack grid [47]. WS_2 (group symbol $P6_3/mmc$, group number 194) was modeled with hexagonal unit cell, using a 20x20x1 grid to sample the Brillouin zone. To avoid artificial interactions between replicas, 15 Å of vacuum were included along the out-of-plane direction. The work of separation (W_{SEP}) is calculated as the opposite of the adhesion energy (E_{ADH}):

$$W_{SEP} = -E_{ADH} = \frac{2E_M - E_B}{A} \quad (1)$$

where E_M is the total energy of the relaxed monolayer, E_B is the total energy of the bilayer in its most favorable configuration, and A is the area of the cell. To evaluate the potential energy surface (PES) we repeated the calculation of W_{SEP} at different relative lateral positions. The potential corrugation (ΔW_{SEP}) rises from the difference between the maximum and minimum W_{SEP} of the PES (i.e., $\Delta W_{SEP} = W^{max} - W^{min}$). Details about the lateral positions used to construct the PES and about calculations underload can be found in the Supporting Information.

3. Results and discussion

3.1. Characterization of the TMCCs

The TMCC powders studied here are multilayered, featuring a transition metal carbide core and chalcogen surface chemistry (Fig. 1a). They exhibit strong intralayer bonding (covalent/ionic) and weak out-of-plane vdW forces between layers, allowing atomic layers to slide easily due to shearing. Nb_2S_2C and Ta_2S_2C multilayer powders were synthesized using a simple and scalable powder metallurgy process, followed by a chemical treatment to remove excess Fe (FeS was used as the source of S during synthesis). **Fig. 1b** presents SEM images of Nb_2S_2C and Ta_2S_2C multilayer particles and EDS elemental maps of Nb/Ta, S, and C, confirming uniform distribution. The Fe signal remains quite intense, despite the use of various etching trials to reduce the iron content [26]. Indeed, EDS quantitative analysis revealed ratios of Nb:Fe = 2.00:0.14 ± 0.06 and Ta:Fe = 2.00:0.31 ± 0.01, indicating incomplete Fe removal. However, to date, there are no reports in the literature of successfully achieving complete Fe removal from TMCC multilayers using hydrochloric acid etching. The average particle size of Nb_2S_2C is 16.7 ± 3.06 μm, while for Ta_2S_2C the average particle size is 11.0 ± 4.57 μm. XRD patterns in **Fig. 1c** confirm the successful phase formation of Nb_2S_2C and Ta_2S_2C after chemical treatment, although secondary phases such as Nb_2SC, NbC, and TaC were also observed. The lattice parameters of TMCCs have been determined from the recorded powder x-ray diffraction patterns [26]. The crystal structure of TMCCs is trigonal

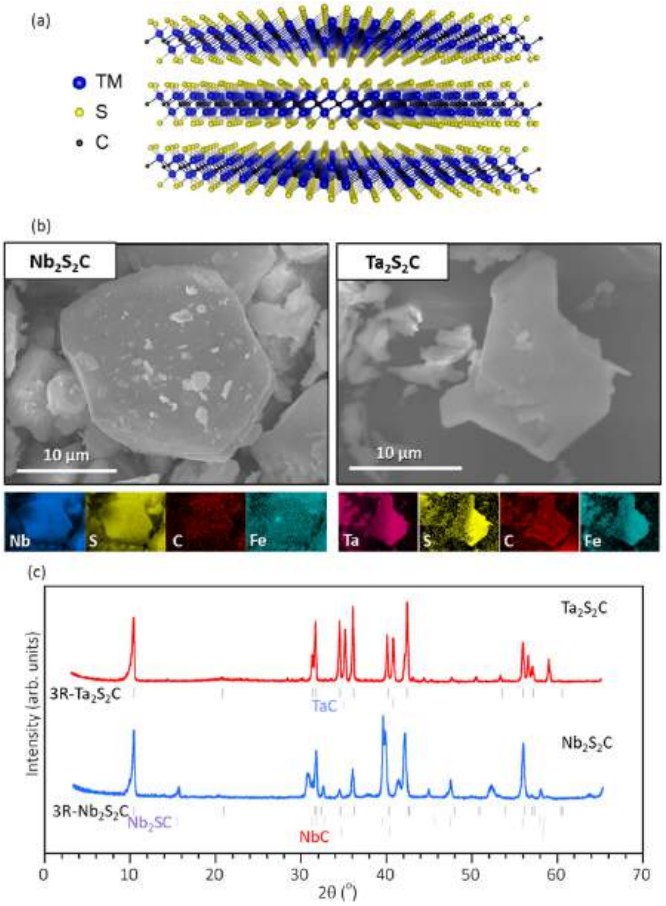

Fig. 1. Multilayer TMCC powders: (a) Schematic for the typical atomic structure of TMCC showing layered morphology, (b) SEM images of Nb_2S_2C and Ta_2S_2C particles in addition to EDS elemental map of Nb/Ta, S, C, and Fe. (c) XRD pattern of Nb_2S_2C with references of 3R–Nb_2S_2C PDF#01-070-8925, Nb_2SC PDF#00-021-0604, NbC PDF#01-070-8416, 3R–Ta_2S_2C PDF#00-024-1258, and TaC PDF#03-065-8264. (A colour version of this figure can be viewed online.)

with space group symbol $R\bar{3}m$, the lattice parameters in the x, y, and z directions are denoted as a, b, and c, respectively, with $a = b$. For Nb_2S_2C, a and c are 3.31 Å and 26.68 Å, respectively, while for Ta_2S_2C a and c are 3.29 Å and 26.59 Å, respectively. Since three TMCC layers are stacked within a single unit cell, the resulting interlayer distance is approximately 8.88 Å, calculated by dividing the c vector by three. Further visualizations of the TMCCs crystal structure are provided in Fig. S1 of the Supporting Information. The XPS analysis of the as-synthesized TMCCs nanolayers was conducted and reported in our previous work [26], where Nb, S, and C peaks were detected, while no Cl signal from HCl etching was observed in neither TMCCs.

3.2. Frictional performance of the TMCCs

We assessed the tribological performance of the different as-synthesized TMCC multilayer powders on a ball-on-disk tribometer in linear sliding mode. Fig. 2a demonstrates the evolution of the COF of TMCC samples (viz., Ta_2S_2C and Nb_2S_2C) against counterbodies (CBs) of different nature: Al_2O_3, SiC and PTFE, to assess the dependence of TMCC's tribological performance on the material pairing. Their frictional behavior is compared to a steel reference sample without the addition of any lubricating material.

Concerning the steel sample against the Al_2O_3 counterbody without the addition of TMCC powders, we observe the typical behavior of a non-lubricated metal surface sliding against a ceramic counterbody, with pronounced fluctuations during the running-in period and a rapidly rising COF [48]. Specifically, the COF started at around 0.4 and quickly increased during the first 500 s, after which the COF remained steady and stable between 0.7 and 0.8. On the other hand, TMCC-lubricated surfaces started at a much lower COF of ~0.15. Afterwards, the COF slightly increased constantly but remained overall low (around 0.2) throughout the entire measuring duration of 1800 s, almost identically for both Ta_2S_2C and Nb_2S_2C. These low COF values are astonishing especially since they were achieved by simply adding lubricious material in the form of powders to the contact area, without the need of a coating process. This unambiguously confirms the lubricant potential of the multilayer TMCC powders, especially considering that the COF is mostly below 0.2. The wear track morphologies after the tribo-tests with Al_2O_3 CB are reported in the bottom part of Fig. 2 for (**b**) the reference case, (**c**) Nb_2S_2C and (**d**) Ta_2S_2C. Height maps of the same areas are also provided beneath the optical images in addition to profiles along the dashed lines (Fig. 2e–j). Significant abrasion marks were found when the Al_2O_3 ball was rubbed against the steel plate without the addition of any lubricious material. This was also clearly observed in the depth profiles (Fig. 2e) and height maps (Fig. 2h), which showed wear up to a maximum depth of ~0.5 µm in addition to the debris pile up at the reversal point as well as along the sides of the wear track. Conversely, no wear was detected in the TMCC-lubricated steel substrate (Fig. 2f and g). Instead, volume build-up along the wear track length can be observed due to the formation of a protective layer, thus preventing the direct contact between the tribo-pair. This holds true for the case of Nb_2S_2C powder, where a patchy tribofilm covered the substrate all along the wear track. For Ta_2S_2C, the tribofilm appeared less thick and patchier; although showing some discontinuities and reduced compactness, such a layer was sufficient to prevent abrasive wear, since no remarkable wear scar can be identified inside the wear track. Similar tribofilm morphologies have been found for other loosely bound solid lubricant films [15,32]. Height profiles across the Nb_2S_2C- and Ta_2S_2C-based tribofilms (Fig. 2i and j) highlight their similar shape with a concave form resulting from the ball's shape. The formation of the protecting tribofilm relates to the uncontrolled compacting of TMCC powder over the substrate, thanks to the mechanical force exerted by the counterbody. Therefore, the morphology and thickness of the resulting tribofilm were somehow affected by stochastic parameters (e.g., the amount of TMCC particles in the contact area and their size). That would explain the minor differences observed between Nb_2S_2C and Ta_2S_2C, as well as small deviations between various repetitions (shown in Fig. S2).

Clearly, the tribological performance greatly depends on the used CB (Fig. 2a). The COF was found to be generally low and quite stable when using Al_2O_3, SiC and PTFE. While Ta_2S_2C and Nb_2S_2C demonstrate nearly identical frictional behavior when using an Al_2O_3 CB, the friction values increase significantly faster for Nb_2S_2C in case of the SiC CB. This indicates a tribofilm with lower adhesion and, therefore, faster removal from the contact area.

In case of the PTFE CB, friction was even higher than the reference sample, which can be associated to the friction reducing effects of PTFE [49]. While this might seem like a negative result at first, it is nonetheless clear proof of the formation of a tribologically active tribofilm composed of TMCC, which shields the rubbing surfaces and accommodates shear. This shielding is why PTFE cannot be effective as a lubricating material and the COF of the tests with the TMCC powder is higher, in fact almost identical to the tests with the Al_2O_3 CB.

Images of the wear tracks were profiled by laser scanning microscopy for each of the considered materials are shown in Fig. S3. Al_2O_3 (Fig. 2e–j) and SiC (Fig. S3a) lead to indiscernible tribofilms of similar compactness and thickness. For the PTFE counterbody, the resulting film was much less compacted (Fig. S3b), although it effectively hosted the sliding interfaces (same COF trend). The less compacted film when using PTFE can be explained by the much smaller acting contact pressure due to the lower elastic modulus of PTFE. Interestingly, a tiny abrasive scar was also visible in the upper part of the wear track. Since PTFE is not

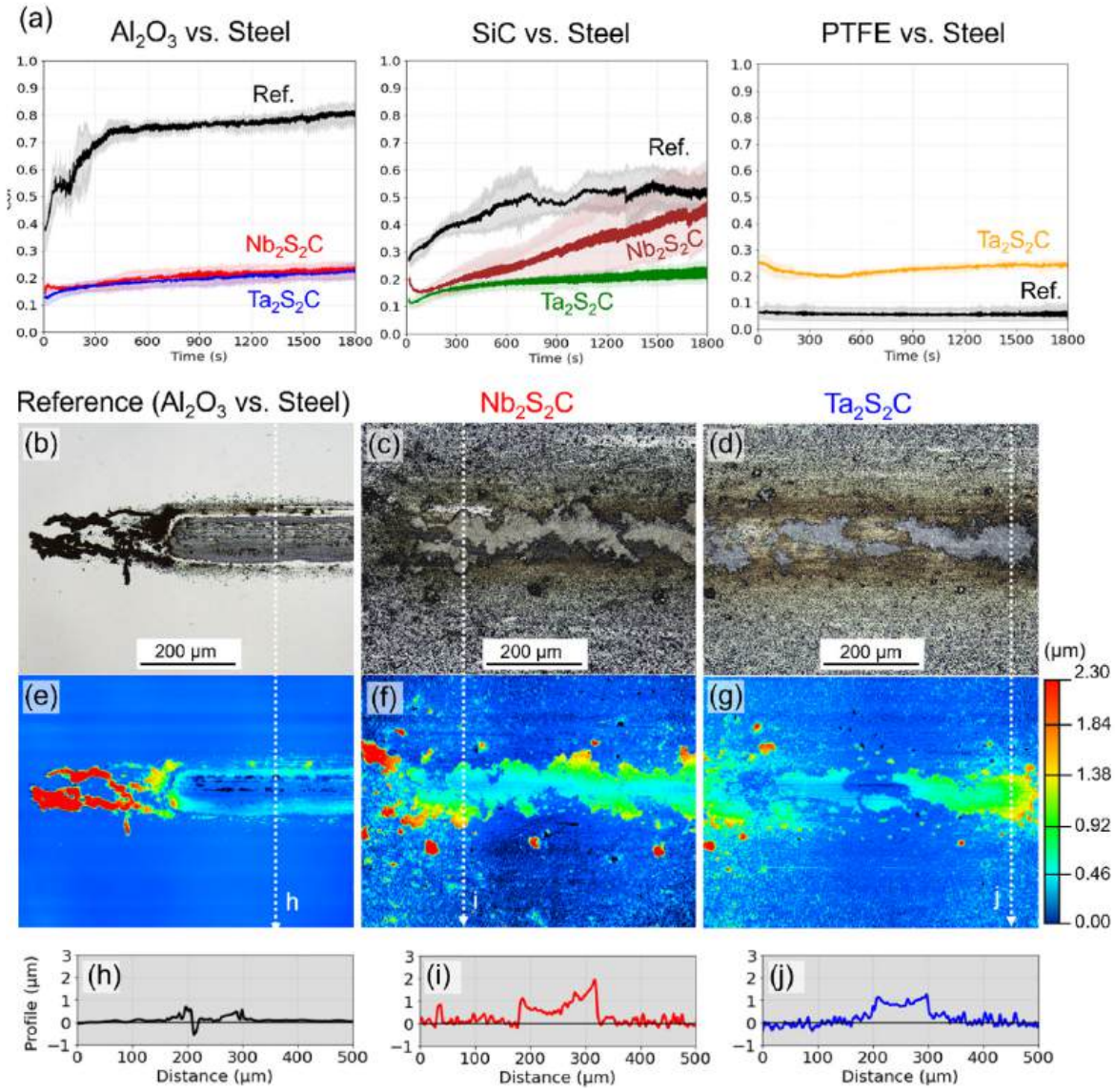

Fig. 2. (a) Tribological performance of Ta_2S_2C and Nb_2S_2C powders against an Al_2O_3 (left), SiC (middle) and PTFE (right) counterbodies. (b–d) laser scanning microscopies and (e–g) corresponding depth profiles of the wear tracks of Al_2O_3 vs. steel, for the reference and TMCC cases. (h–j) 1D cross-section height profiles acquired along the white dashed lines. (A colour version of this figure can be viewed online.)

hard enough to scratch the steel substrate, such abrasion may be traced back to the direct action of TMCC particles. In summary, the morphology of the TMCC-based tribofilm seems to be affected by the Hertzian contact pressure induced by the paired material, i.e., 0.45 GPa for Al_2O_3, 0.48 GPa for SiC, 0.40 GPa for 100Cr6 and only 0.012 GPa for the PTFE CBs.

We also carried out experiments with a 100Cr6 steel CB, suggesting very little beneficial effects of the lubricious Ta_2S_2C powders (Fig. S3c). Indeed, the COF starts very low (~0.2) and increases to the reference value after a few initial cycles, coinciding with the removal of the TMCC powders from the tribological contact. Such behavior is confirmed by deep abrasion marks covering the entire wear track (Fig. S3c). Moreover, the accumulation of debris at the reversal points and around the entire perimeter confirms the occurrence of pronounced abrasive processes, typical of a steel-steel contact. The observations made for the wear behavior and the trend of the friction values strongly indicate that the adhesion of the Ta_2S_2C powder to the steel CB is much lower compared to the ceramic CBs, resulting in a significant reduction in the wear life of the tribofilm.

Overall, the results with the different CBs suggest that both adhesion to the CB and contact pressure play a role in the formation of beneficial TMCC tribofilms. In case of high adhesion of the TMCC powders to the CB (such as for Ta_2S_2C to Al_2O_3 or SiC), the powders remained in contact during tribological testing, forming a beneficial tribofilm. Meanwhile, the low contact pressure for the PTFE counterbody did not efficiently densify the TMCC powders on the substrate, resulting in a less compacted tribofilm. On the other hand, if adhesion to the counterbody was weak, as in the case of the steel CB, the lubricious powders were easily carried out of the contact zone, leading to high friction. We hypothesize that using TMCCs in the form of a coating instead of weakly adhered powder may help improve adhesion to both the substrate and the counterbody, thus extending the applicability of this new 2D material family.

To further confirm the formation of TMCC tribofilms and to understand the underlying tribological mechanisms we carried out multiple analyses of the substrate surfaces after sliding. To provide a complete picture in terms of both chemical composition and structural features, in the following paragraphs we report the results from SEM-EDS, XPS,

AMES, and TEM. As the most promising results were obtained during sliding against an Al_2O_3 counterbody, we focused subsequently on this tribo-pair.

3.3. Wear track analysis

Elemental map overlays by EDS inside the AMES system provide more information about the distribution of the elements inside the tribofilms (Fig. 3). More information on the measurements' position inside the wear tracks can be found in Fig. S4. The SEM images and the elemental mappings of the EDS analysis clearly show the formation of a patchy tribofilm for both Nb_2S_2C and Ta_2S_2C, which is often found for solid lubricant coatings [32,50]. The SEM/EDS images demonstrate that the tribofilms were basically composed of compacted flake-like particles similar in size structure and size to the original powder. The overlaid elemental mappings for Nb_2S_2C (Fig. 3a) and Ta_2S_2C (Fig. 3b) verify that the patches inside the tribofilms were mainly composed of Nb/Ta and S, with only minor contributions of oxygen. Outside the wear tracks the iron signal from the steel substrate prevailes, while no iron can be detected through the tribofilm (Fig. 3c and d). Interestingly, the Fe signal in the EDS mapping was quite intense for the as-synthesized TMCCs (Fig. 1b), but it was not detected in the tribofilm after the sliding experiment. This suggests that the residual Fe may be loosely bonded to the TMCCs and therefore easily removed during friction.

These results conclude that the TMCCs added to the contact area as powders were compressed to form a relatively thick tribofilm, whose functionality did not rely on any specific tribochemical reactions. The fact that no significant oxygen and iron contributions appeared in the EDS measurements inside the tribofilm underscores the stability of the TMCC particles and suggests that a protecting tribofilm was formed preventing tribochemical wear of the substrate.

Further chemical analysis was performed by XPS and AMES to characterize the chemistry of the wear tracks in detail, specifically capturing the surface chemistry and the chemical bonding environments. XPS spectra with the corresponding deconvolution fits for the Nb3d (Ta4f), S2p, C1s and O1s peak areas are shown in Fig. 4 (For more details see Table S1) for (a) Nb_2S_2C and (b) Ta_2S_2C. Nb3d (Ta4f) regions confirm the presence of TMCCs inside the tribofilm, since we observed the presence of doublets centered at 202.8 eV (23.7 eV) in accordance with S–Nb–C (S–Ta–C) chemical bonds [26]. Moreover, the TMCC presence is also highlighted by peaks centered around 160.8 eV in the S2p region and at 284.3 eV inside the C1s region, all related to the S–Nb (Ta)–C bond. It is also worth noting a doublet connecting with metallic tantalum (22.2 and 24.2 eV inside the Ta4f region), that was also reported in Ref. [26] from the XPS analysis on the delaminated TMCCs. The presence of Ta(0) signal in Ta_2S_2C is not clear. It may be connected with the presence of unreacted Ta and TaC from the TMCC synthesis (as observed in Fig. 1b) and/or it may be related to surface defects and damage caused by ion-sputtering. Inside the sulfur region, chemical states involving oxygen are also clearly visible (peak located at 162.3 eV related to SO_x and a small contribution of sulphates around 168.3 eV). Similarly, inside the O1s region we detected the presence of metal oxides (529.7 eV) and carbon-oxygen bonds (531.3 eV). Together with the peaks of C–Nb(Ta)–S at 284.3 eV, the C1s signals reveals four additional components: adventitious carbon (285 eV), C–O (286.4 eV) and C═O (288.2 eV), as well as small amounts of carbide (282.3 eV). Interestingly, almost negligible oxygen signal was observed in the SEM-EDS mapping, whereas from XPS analysis, whose depth typically reaches only up to

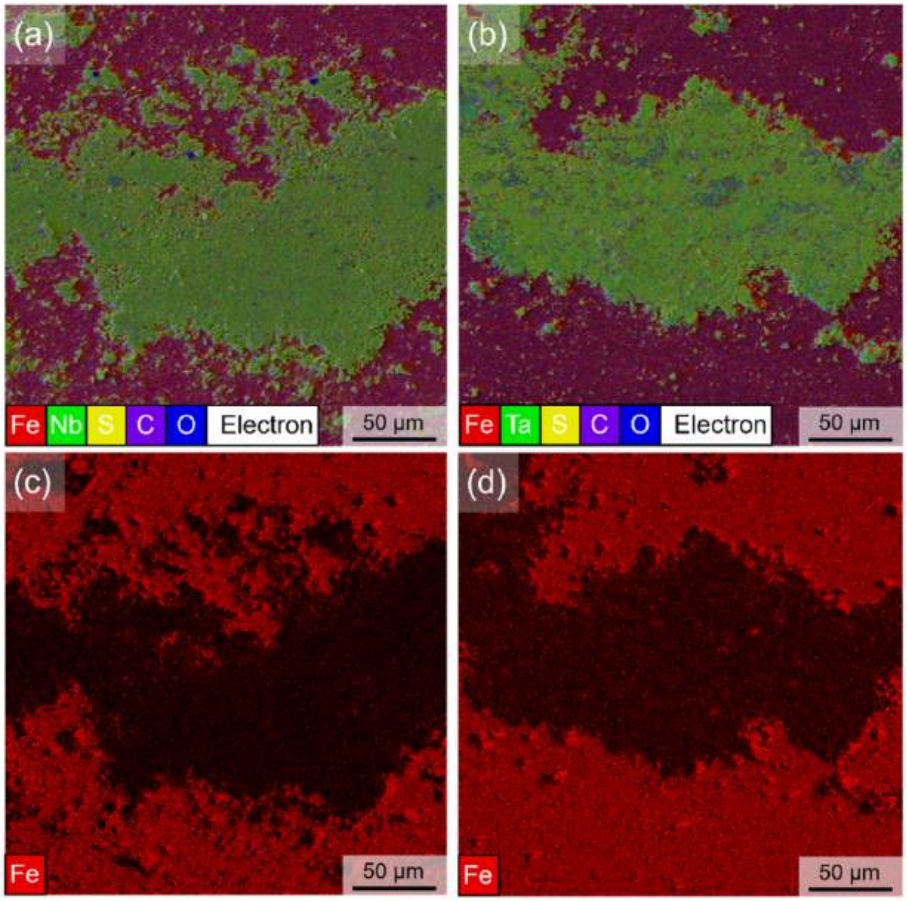

Fig. 3. EDS/SEM elemental map overlays (Fe, Nb/Ta, S, O, C) of tribofilms Nb_2S_2C (a) and Ta_2S_2C (b). Elemental map of Fe to show coverage of the tribofilm on Nb_2S_2C (c) and Ta_2S_2C (d). (A colour version of this figure can be viewed online.)

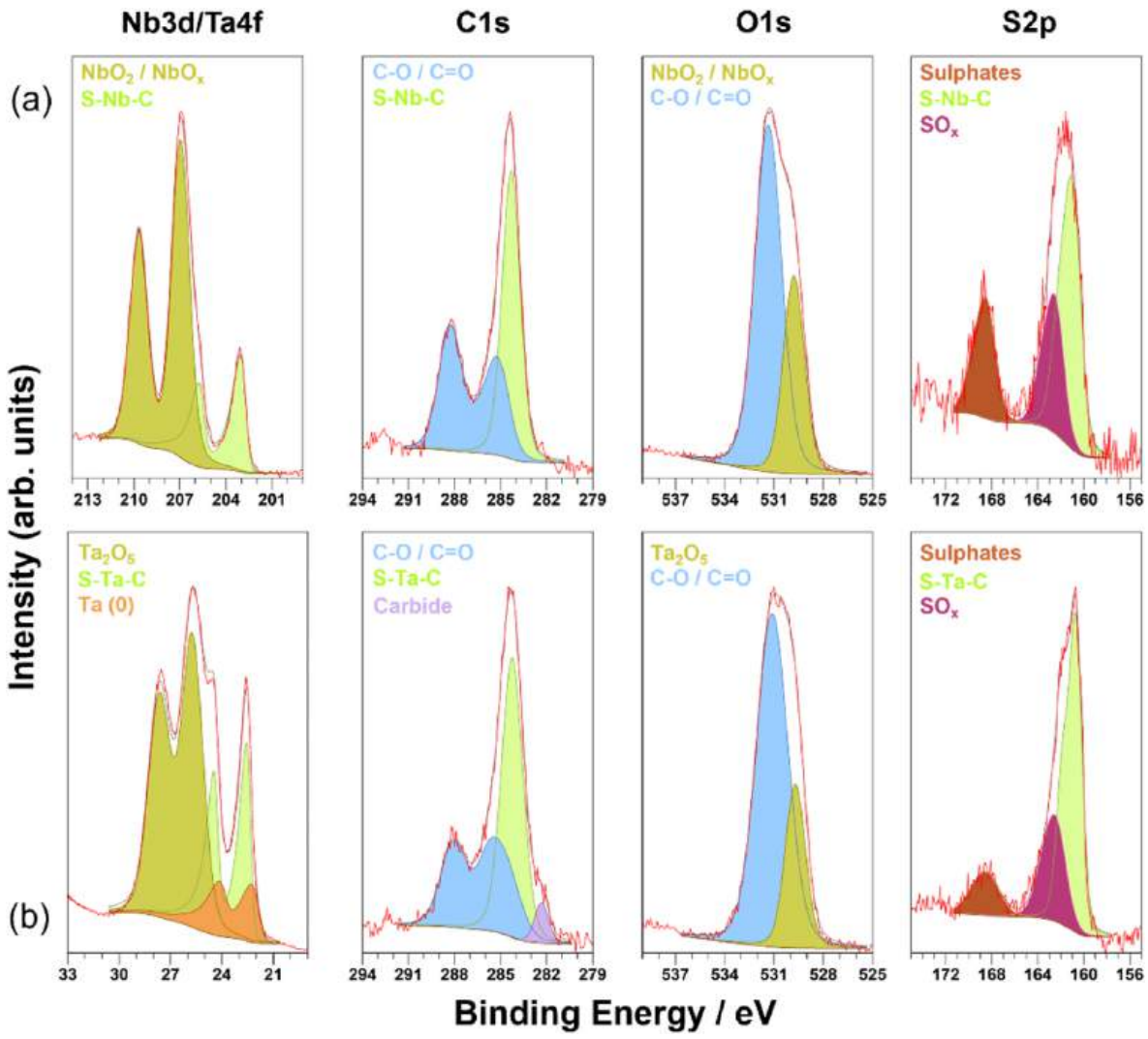

Fig. 4. XPS of the Nb3d/Ta4f, C1, O1s and S2p regions of tribofilms Nb_2S_2C (a) and Ta_2S_2C (b) after surface cleaning. Intensity scales are normalized to the maximum signal for each of the elements. Color code: light green S–Nb/Ta–C, olive (Metal oxide), blue (C, O-contamination), magenta (SO_x), dark orange (sulphates), violet (carbides). (For interpretation of the references to colour in this figure legend, the reader is referred to the Web version of this article.)

7–10 nm, oxygen bonding environments are evidenced. Therefore, we can assume that oxidation is limited exclusively to the near-surface region of the particles. The presence of oxides from XPS analysis may suggest that oxidative reactions happened during rubbing, although traces of native oxides can be observed even without tribological testing [26]. Since the experiments were conducted in air environment, rich in O_2, it is reasonable to believe that oxide layers are repeatedly removed and re-formed.

AMES results are included in Fig. S5 (and Table S2) for (a) Nb_2S_2C and (b) Ta_2S_2C, referring to similar areas analyzed by SEM-EDS (Fig. S4). All the expected elements (Nb, Ta, S, C) were detected, confirming once again the presence of TMCC inside the tribofilm. From Table S2, the oxygen contribution was almost negligible, while the iron signal originated from the underlying steel substrate. Both XPS and AMES/EDS confirm the presence of the expected elements in compacted tribofilms with a thickness of at least 1 μm (deduced from the absence of the iron signal from underneath the tribo track in EDS). The bonding environments found in powder TMCC samples can also be detected in the tribofilms, which allows us to assume that most of the TMCC remains stable. However, small changes are found when compared to Ref. [26] in increased amounts of Nb/Ta/S oxide and the formation of small amounts of sulphates and carbides on the particle surface.

To gain structural and morphological insights into the tribofilm after the friction experiments, we first prepared a FIB cross-section in a representative wear track and performed TEM analysis on it afterwards. The FIB cut on a Nb_2S_2C-based TMCC tribofilm was done on a specific area (Fig. 5a), so that both loose and compacted parts of the tribofilm were included inside the same TEM-lamella (Fig. 5b and c). The cross-sectional view of the compacted tribofilm area (Fig. 5d) reveals a flat tribofilm with a homogeneous thickness of about 1 μm. The voids observed are mainly generated by the thinning process during FIB processing, since originally the tribofilm appeared fully dense consisting of TMCC particles of different sizes, including micron sized large TMCC particles with a low degree of wear, as well as powders that have been frictionally ground down to the nanoscale. Selected area electron diffraction (SAED) in Fig. 5e–g highlights that the large micron-sized TMCC particles have a crystalline structure, while the smaller-sized particles exhibit mainly nanocrystalline and amorphous phase diffraction patterns. The Nb_2S_2C presence is clearly confirmed by the subsequent EDS mapping (Fig. 5h), where Nb, S, C, and O are detected. Interestingly, no significant oxidation occurred inside the larger TMCC particles, while the oxygen signal is more intense for those areas surrounding the particle surface. This is in accordance with the assumption that tribochemical reactions are more pronounced at the locations with more wear.

The high-resolution TEM morphology of the tribofilm is reported in

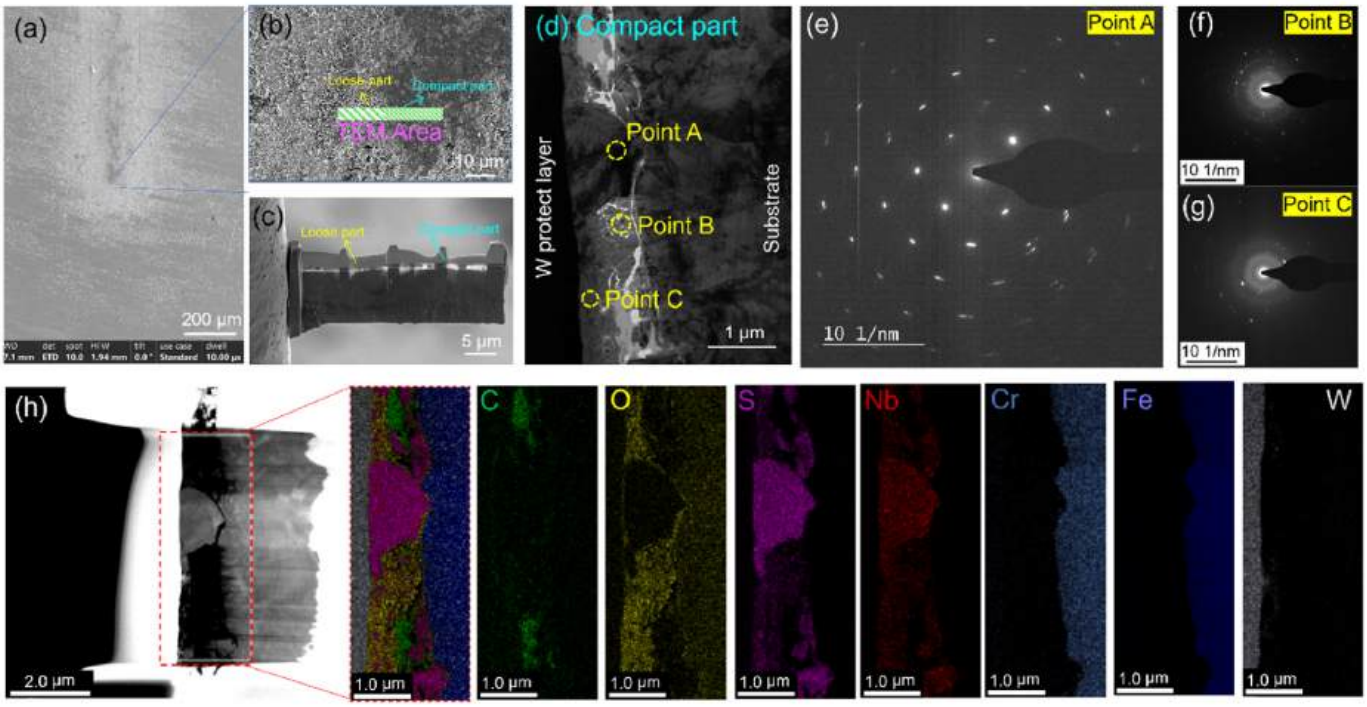

Fig. 5. TEM results for Nb_2S_2C powder after sliding: (a–c) FIB lamella preparation, (d) cross-sectional morphology of the compacted part of the tribofilm inside the wear track, (e–g) corresponding SAED patterns at different positions, and (h) EDS mapping results. (A colour version of this figure can be viewed online.)

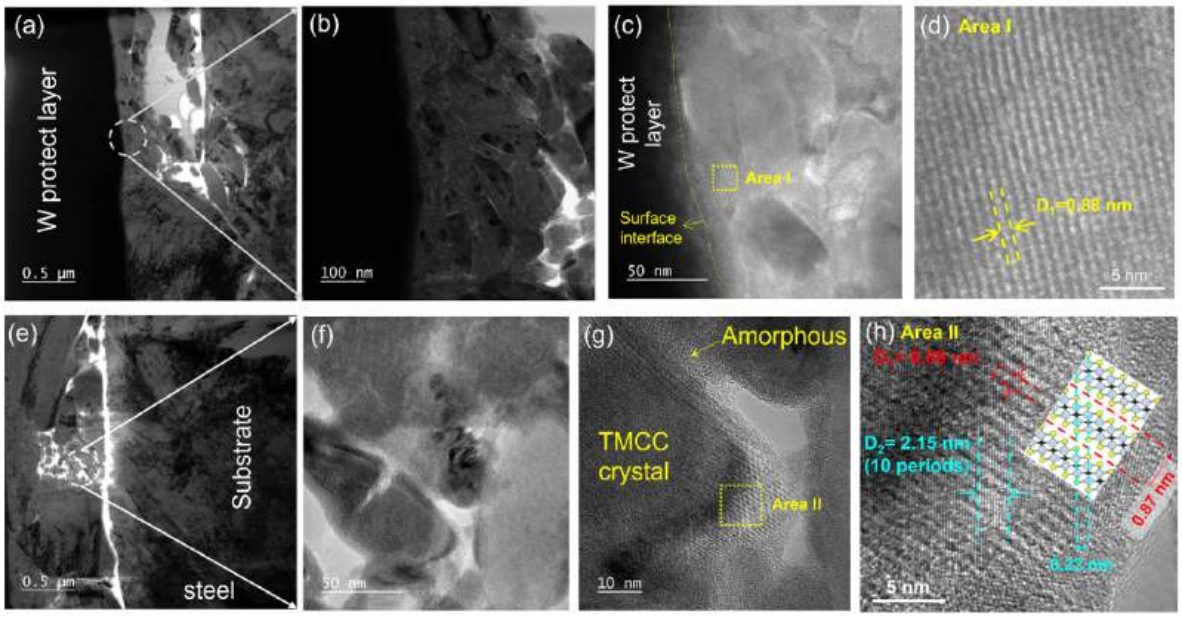

Fig. 6. TEM results for Nb_2S_2C powder after sliding: (a–b) TEM images of the near-surface region of the wear track and (c–d) corresponding high-resolution TEM images of the TMCC particle near the surface. TEM images of the region close to the substrate (e–f) and corresponding (g–h) high-resolution TEM images of the small TMCC particles. The inset inside panel (h) shows the crystal structure of Nb_2S_2C simulated in this work, as well as the observed interplanar distances. (A colour version of this figure can be viewed online.)

Fig. 6. In the region close to the surface of the tribofilm, the TMCC layers show a distribution trend parallel to the surface (Fig. 6c and d). The measured interlayer distance is about 0.88 nm, which connects well with the {001} Nb_2S_2C crystal plane. These 2D TMCC planes are the ones with weak interacting forces and, therefore, they are the ones supposed to accommodate interlayer sliding. Such evidence can explain the excellent tribological performance observed for the TMCC powder. In addition, Fig. 6e–h shows high-resolution images of some small particles inside the tribofilm, highlighting the presence of an amorphous phase embedding these particles. From the TEM-EDS results of Fig. 5, it seems that such amorphous phase is composed of oxides, most likely originated from the particle's surface during the tribological process and pressed together with unoxidized Nb_2S_2C layers [50]. The high-resolution image of TMCC small particles (Fig. 6g) reveals a crystalline interior where the {001} and {012} crystal planes are clearly visible (Fig. 6h). The interlayer distances measured based on HR-TEM are almost identical to the

simulated values for Nb_2S_2C (inset in Fig. 6h). These results confirm that the tribofilm is mainly composed of unoxidized TMCC crystalline nanoparticles, embedded in an oxide-based amorphous matrix. Compared with TMD materials, TMCCs seem to have higher thermal and chemical stability, which may be traced back to the strong Nb–C bonds. Because they are more chemically inert, oxidative processes are limited to the outermost TMCC layers. However, the presence of an oxidic phase inside the tribofilm is not necessarily negative, as it may help prevent the rapid exfoliation of TMCCs flakes. More studies are needed to investigate the role of oxides, whether they are also lubricious or have a mere retention function.

3.4. Interlayer sliding of TMCCs by DFT simulations

TEM-EDS analysis confirms the presence of intact and crystalline 2D TMCC layers within the effective tribofilm. Supported by this experimental evidence, we carried out numerical DFT calculations to model the interlayer sliding for Nb_2S_2C and Ta_2S_2C bilayers, exploring their easy-to-shear properties from a nanoscale perspective. The amount of energy required to separate two layers, i.e., the work of separation (W_{SEP}), and the potential corrugation values (ΔW_{SEP}) are listed in Table 1. These two quantities represent a good predictor for the lubricating ability of materials [51,52], since they correlate with the shear strength [53]. In addition to Nb_2S_2C and Ta_2S_2C, we also provide a comparison with well-established solid lubricants, i.e., MoS_2, graphene, WS_2 and Ti_2CT_x (T = $F_{1/3}$, $O_{1/3}$, $OH_{1/3}$). The low W_{SEP} and ΔW_{SEP} values observed for Nb_2S_2C and Ta_2S_2C connect well with the vdW nature of their interlayer interactions. Ta_2S_2C (0.33 J/m^2) shows a slightly higher binding energy than Nb_2S_2C (0.24 J/m^2), since electronic correlation effects are more pronounced for Ta than Nb, leading to stronger Van der Waals interactions. However, the maximum energetic barriers experienced during mutual sliding are almost the same for the two TMCCs (ΔW_{SEP} = 0.08–0.10 J/m^2), being in the range observed for graphene, MoS_2 and WS_2 [54]. The comparison between TMCCs and titanium-based MXenes (Ti_2CT_x) strictly depends on the termination types of MXene (T), which are known to be poorly controllable when following a top-down HF etching approach [55]. As documented by some of the authors [46], MXene layers with mixed terminations have a significant interlayer adhesion (0.52 J/m^2), due to the formation of hydrogen bonds and dipole-dipole interactions between layers, making them more adhesive to each other and reducing the interlayer slipperiness. Nb_2S_2C and Ta_2S_2C layers, conversely, only expose to the interface homogeneous sulfur terminations, leading to pure vdW forces acting between the layers and hence low interlayer adhesion. Although MoS_2 and WS_2 layers are also passivated by sulfur atoms, Nb_2S_2C and Ta_2S_2C exhibit lower ΔW_{SEP} values, suggesting better performance for TMCCs, at least in principle. It is important to note that DFT calculations presented here serve as an ideal predictive tool and do not account for other potentially significant factors acting at the micro- and macro-scales (surface roughness, grain boundaries).

To further confirm the lubrication ability of TMCCs, in Fig. 7 we report the potential energy surface (PES) for Nb_2S_2C and Ta_2S_2C bilayers as a function of the external load applied (from 0 to 5 GPa). Since a PES describes the interlayer interaction between two surfaces as a function of their relative lateral position, it provides precise information about the energetic barriers experienced during mutual sliding, or in other words, about the amount of energy that can be dissipated by frictional processes. Both Nb_2S_2C and Ta_2S_2C show hexagonal crystal structure with similar *a* lattice parameter (3.284 Å and 3.268 Å, respectively, in very good agreement with Ref. [26]) and the same most favorable stackings (labeled 'min 1' and 'min 2' in Fig. 7). The minimum energy path (MEP, i.e., the most favorable sliding path during reciprocal sliding) is highlighted with a yellow dashed line, while the corresponding energy profile is reported on the right side of Fig. 7. The energy barriers faced during interlayer sliding along the MEP are surprisingly low, with almost no difference between Nb_2S_2C and Ta_2S_2C. Indeed, for applied normal loads ranging from 0 to 5 GPa the maximum energy barrier never exceeded 0.05 J/m^2. Such numerical results are in perfect agreement with our experimental findings as they confirm the easy-to-shear ability of TMCCs. Moreover, they predict a similar lubricant behavior between Nb_2S_2C and Ta_2S_2C, which has also been observed in our experiments whenever the TMCC-based tribofilm was formed.

Table 1
Work of separation (W_{SEP}) and Potential Energy Surface corrugation (ΔW_{SEP}) values for a selected list of 2D materials.

2D-bilayer	W_{SEP} (J/m^2)	ΔW_{SEP} (J/m^2)
Nb_2S_2C	0.24	0.08
Ta_2S_2C	0.33	0.10
Graphene	(0.25)[a]	(0.06)[a]
	(0.26)[b]	(0.08)[b]
MoS_2	(0.26)[a]	(0.12)[a]
	(0.27)[b]	(0.10)[b]
WS_2	0.29	0.12
Ti_2CT_x (T = $F_{1/3}$, $O_{1/3}$, $OH_{1/3}$)	(0.52)[a]	(0.46)[a]

[a] Ref. [46].
[b] Ref. [54].

3.5. Comparison with WS_2 and $Ti_3C_2T_x$

So far, we have widely discussed the tribological performance of TMCC powders in both reducing the COF and preventing wear. While no complicated coating process had to be applied, but the TMCCs were simply added to the contact area in powder, the results were still impressive. The exceptional tribological performance can be traced back to their ability to form an adhesive and protective tribofilm, where the TMCC layers are oriented in parallel to the surface. Once the TMCC-based tribofilm is formed, the 2D nature of the Nb_2S_2C/Ta_2S_2C flakes ensures easy shearing, thus leading to low friction. Therefore, to further highlight the remarkable performance of the used TMCC powders (Nb_2S_2C and Ta_2S_2C) in reducing the COF, in Fig. 8 we report on the results we obtained for WS_2 and $Ti_3C_2T_x$ MXene as-deposited powders under the same tribological conditions as described before against Al_2O_3 counterbody, i.e., Hertzian contact pressure of 0.45 GPa, stroke length of 1 mm and sliding velocity of 1 mm/s.

Fig. 8 clearly indicates that Nb_2S_2C and Ta_2S_2C outperform WS_2 and $Ti_3C_2T_x$ powders in terms of frictional performance. It is worth mentioning that WS_2 and $Ti_3C_2T_x$ are usually not tested as powders, instead they are commonly applied as coatings to optimize their performance. However, the resulting COFs from Fig. 8 are close to earlier observed values when WS_2 or $Ti_3C_2T_x$ were applied as coatings and tested under similar conditions [33,56,57]. In the first few minutes, the WS_2 powder could efficiently lubricate the tribological contact, leading to COF similar to the TMCCs. The standard deviation (e.g., highlighted by the faded area in the diagram) reaches even values well below the limit of 0.2 observed for TMCCs. However, after a while the WS_2 powders were rapidly removed from the contact, with the effect that the COF reached the reference value. Instead, $Ti_3C_2T_x$ powder was completely dislodged from the wear track from the very beginning of the experiments, being indicative of low adhesion to the sliding surfaces. These comparative results highlight the importance for 2D materials of establishing a good adhesion to the substrate, so as to resist the peeling-off during rubbing. Further benchmarking and comparisons with other Niobium- and Tantalum-based TMDs (NbS_2 and TaS_2) or MXenes are expected to enhance the understanding of TMCCs' potential usage as lubricants.

The excellent performance of TMCC powders depicted in this paper, also supported by DFT simulations, demonstrate the easy-to-shearability typical for layered materials in combination with high adhesion to the sliding surfaces. These results will pave the way for further investigations involving more advanced deposition techniques (e.g., air-spraying, electro-spraying) and all sort of tribological testing conditions

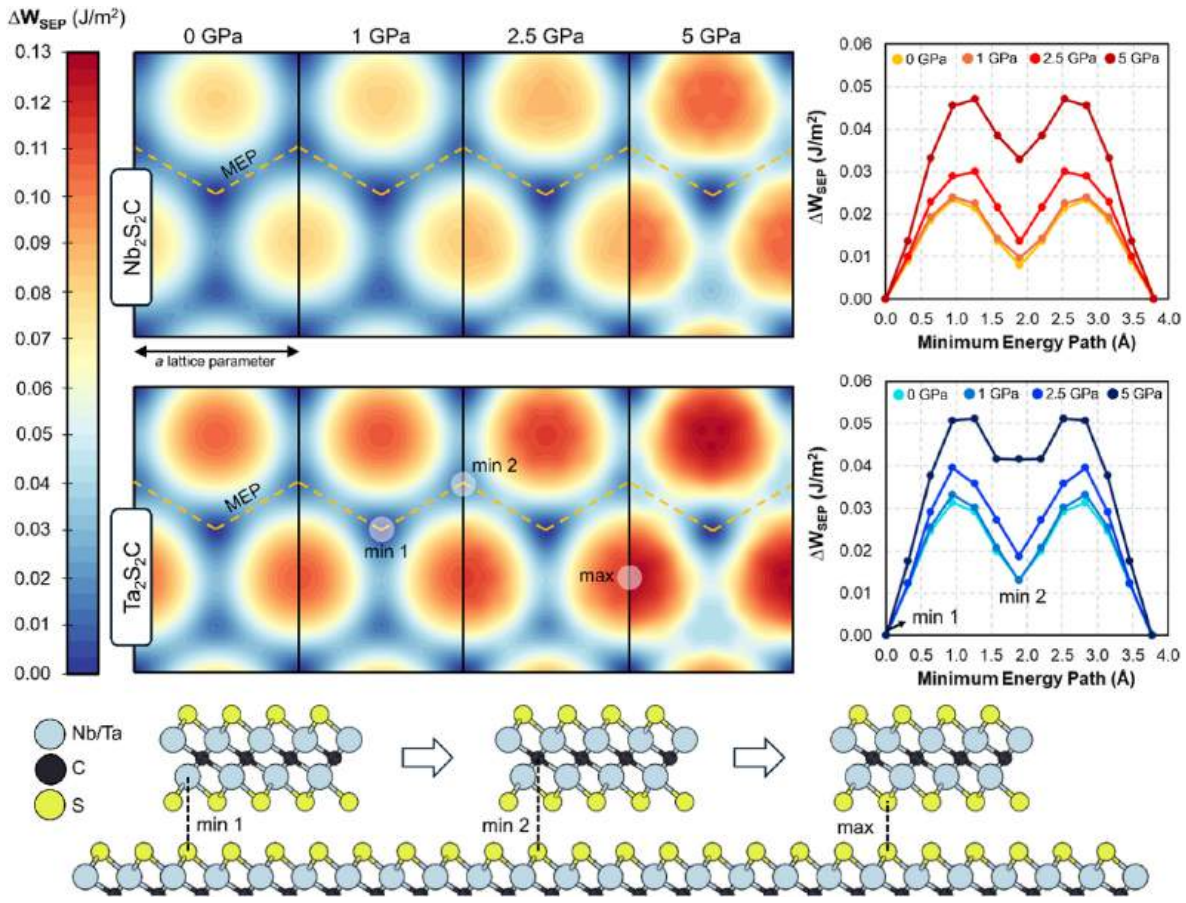

Fig. 7. Potential energy surfaces (PES) for bilayers of Nb_2S_2C (above) and Ta_2S_2C (below) from 0 to 5 GPa load. The minimum energy path (MEP) is highlighted by a yellow dashed line, with the corresponding energy profile depicted on the right. Schematics on the relevant lateral configurations (min1, min2 and max) are shown below the PESes. (For interpretation of the references to colour in this figure legend, the reader is referred to the Web version of this article.)

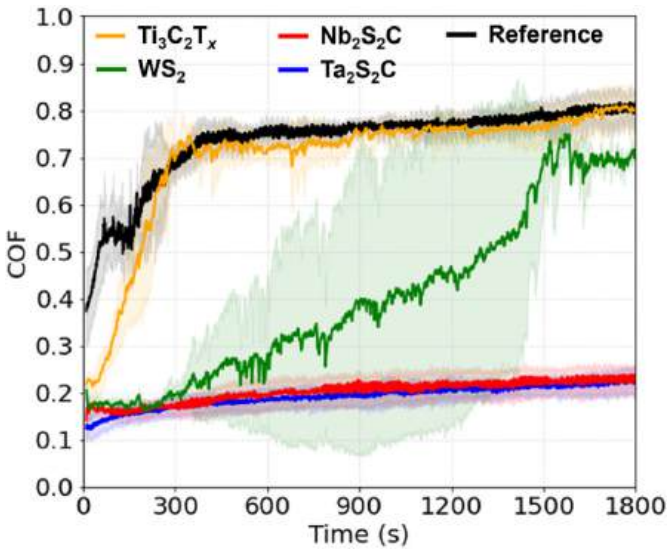

Fig. 8. Tribological performance of Nb_2S_2C (red line) and Ta_2S_2C (blue) TMCCs compared with tungsten disulfide (WS_2, green) and MXene ($Ti_3C_2T_x$, yellow) powders, against Al_2O_3 counterbody. (For interpretation of the references to colour in this figure legend, the reader is referred to the Web version of this article.)

under different environmental conditions (e.g. under nitrogen or vacuum). It is worth noting that the samples tested here contained secondary phases such as rock-salt carbides and MAX phases, which are known to have strong bonding in all directions and lack the weak out-of-plane forces found in TMCC. Thus, it is reasonable to assume that with pure samples, one can predict better lubricity behavior. Therefore, increasing the purity of the vdW-TMCC phase is essential for accurate performance benchmarking against other vdW structures.

4. Conclusions

This research article first aimed at introducing a new 2D layered family of materials namely Transition metal carbo-chalcogenides (TMCCs). TMCCs are until today nearly unexplored in the tribological community but they inherently combine interesting features of TMDs and MXenes thus potentially leading to mechanically and environmentally stable properties when applying them as solid lubricants.

In this work we have broadly discussed the tribological behavior of 2D layered TMCCs (Ta_2S_2C and Nb_2S_2C) when added only as powder onto steel substrates (AISI304), exploring the effect of different counterbody materials (Al_2O_3, SiC, PTFE, and 100Cr6 steel) in a ball-on-disk setup, in ambient air. Overall, in most cases the presence of Ta_2S_2C and Nb_2S_2C in the contact area turned out to be beneficial in terms of effective lubrication, significantly outperforming traditional 2D materials like WS_2 and MXenes as we showed in Fig. 8. Responsible for this was the quick formation of a not continuous but patchy tribofilm due to compacted TMCC powder during rubbing tests against ceramic materials (Al_2O_3 and SiC balls), capable of protecting the tribo-pair from excessive wear and ensuring a stable and low coefficient of friction (COF

<0.2; typical for solid lubricants). For the case of a PTFE counterbody, featuring a much lower elastic modulus, we observed a less compacted but still effective tribofilm (same COF trend). In contrast, when using a steel counterbody, after a few cycles the TMCC powder is completely removed from the substrate, leaving the contact unlubricated. Therefore, we concluded that high adhesion of the TMCC particles to the counterbody and a sufficiently high contact pressure are requirements for the formation of a beneficial tribofilm, as observed for ceramic counterbodies in our study.

The SEM-EDS measurements on the wear tracks revealed that the tribofilms are not continuous and consist of patches out of compacted TMCCs particles (Nb/Ta, S and C signals). Similarly, XPS and AMES analysis of the near-surface region highlighted the proper binding environments (S–Nb/Ta–C) and elements (Nb/Ta, S, C) expected for TMCCs. TEM-EDS imaging coupled with SAED revealed that TMCC particles compacted within the tribofilm have different sizes: large micron-sized particles with a crystalline structure, as well as nanocrystalline smaller-sized particles embedded in an amorphous oxide phase. While SEM-EDS mapping revealed only a negligible amount of oxygen signal, from XPS analysis, whose depth is localized within 7–10 nm, oxygen bonding environments were visible (SO_x, sulphates, metal oxides, C–O, C═O).

From these results we assumed that although oxidative processes occur in the near-surface region, the functionality of the tribofilm does not rely on any highly-transforming tribochemical reactions, but rather on the layered structure of TMCCs, which facilitates easy interlayer shearing. Indeed, the high-resolution TEM images in the near-surface region revealed the presence of TMCC flakes that are oriented parallel to the sliding surface. The low oxidation degree also demonstrates the high environmental stability of the TMCCs under tribological loading in the air environment.

The experimental results are additionally supported by comparative DFT simulations, which demonstrated low energy barriers for interlayer sliding in TMCCs, confirming their potential as efficient solid lubricants.

For the application as solid lubricants, it is finally not only about the absolute value of the COF but also about the capability to mitigate wear and to provide a reliable and easy to apply possibility to lubricate contacts. Superlubricity for example has been shown so far for many different systems, but it still fails on macroscale when used in real machine elements to guarantee a low and reliable friction coefficient without severe wear and the looming ban of PFAS products such as PTFE additionally requires looking further for candidates with an interesting portfolio. However, future research in the field of TMCCs should focus on optimizing the synthesis and application methods, exploring more advanced deposition techniques (e.g., air- or electro-spraying), and conducting comprehensive tribological testing under a wide range of conditions such as higher temperatures or under nitrogen/vacuum environment to further screen this new class of materials. The presented results are a first nucleus to introduce TMCCs to the materials science and in particular tribology community elucidating possibilities for more durable, efficient and sustainable solid lubricants.

CRediT authorship contribution statement

Philipp G. Grützmacher: Writing – original draft, Supervision, Methodology, Investigation, Formal analysis, Data curation, Conceptualization. **Ahmad Majed:** Writing – original draft, Methodology, Investigation, Data curation. **Edoardo Marquis:** Writing – original draft, Methodology, Investigation, Formal analysis, Data curation. **Xudong Sui:** Writing – original draft, Investigation, Formal analysis, Data curation. **M. Clelia Righi:** Writing – original draft, Methodology, Investigation, Data curation. **Markus Sauer:** Writing – original draft, Investigation, Formal analysis, Data curation. **Annette Foelske:** Writing – original draft, Investigation, Formal analysis, Data curation. **Michael Naguib:** Writing – original draft, Supervision, Investigation, Funding acquisition, Formal analysis, Data curation, Conceptualization. **Carsten Gachot:** Writing – original draft, Validation, Methodology, Investigation, Funding acquisition, Formal analysis, Data curation, Conceptualization.

Notes

Authors approve ethics in publishing and consent to participate thereof.

The authors declare consent for publication.

Funding sources

FFG project “ELSA” under grant n° 884672.

European Research Council (ERC) Grant agreement No. 865633 under the project “Advancing Solid Interface and Lubricants by First Principles Material Design” (SLIDE).

LICP International Cooperative Scholarship.

Task 12, Advanced Materials for Transportation – Technology Collaborative Program (AMT-TCP), FFG Project title: 2D materials and laser-based surface processes to increase resource efficiency in mobility applications; Project number: FO999908089; eCall number: 51519652; IEA call for proposals 2023 – KLIEN.

Declaration of competing interest

The authors declare that they have no known competing financial interests or personal relationships that could have appeared to influence the work reported in this paper.

Acknowledgement

Synthesis and characterization of TMCCs at Tulane University was supported by the US National Science Foundation (NSF) CAREER Project DMR-2048164. The Austrian Research Promotion Agency (FFG) is gratefully acknowledged for funding of the XPS and AMES infrastructure (FFG project number: 884672). These results are part of the “Advancing Solid Interface and Lubricants by First Principles Material Design (SLIDE)” project that received funding from the European Research Council (ERC) under the European Union’s Horizon 2020 research and innovation program (Grant Agreement No. 865633). EM and MCR acknowledge the CINECA award under the ISCRA initiative, for the availability of high-performance computing resources and support.

Appendix A. Supplementary data

Supplementary data to this article can be found online at https://doi.org/10.1016/j.carbon.2024.119695.

References

[1] C.A. Mirkin, E.H. Sargent, D.P. Schrag, Energy transition needs new materials, Science. 384 (2024), 713–713.
[2] V. Agarwal, S. Agarwal, Performance profiling of solid lubricant for eco-friendly sustainable manufacturing, J. Manuf. Process. 64 (2021) 294–305.
[3] T.W. Scharf, S.V. Prasad, Solid lubricants: a review, J. Mater. Sci. 48 (2013) 511–531.
[4] S. Zhang, T. Ma, A. Erdemir, Q. Li, Tribology of two-dimensional materials: from mechanisms to modulating strategies, Mater. Today 26 (2019) 67–86.
[5] D. Berman, A. Erdemir, A.V. Sumant, Approaches for achieving superlubricity in two-dimensional materials, ACS Nano 12 (2018) 2122–2137.
[6] H.A. Zaharin, M.J. Ghazali, N. Thachnatharen, F. Ezzah, R. Walvekar, M. Khalid, Progress in 2D materials based nanolubricants: a review, FlatChem 38 (2023) 100485.
[7] Y. Guo, X. Zhou, K. Lee, H.C. Yoon, Q. Xu, D. Wang, Recent development in friction of 2D materials: from mechanisms to applications, Nanotechnology 32 (2021) 312002.
[8] M.Z. Baykara, M.R. Vazirisereshk, A. Martini, Emerging superlubricity: a review of the state of the art and perspectives on future research, Appl. Phys. Rev. 5 (2018) 041102.
[9] https://www.dicronite.com/tungsten-disulfide/; https://www.dicronite.com/mars-explorer/. *accessed 16 July* **2024**.

[10] R. Lince Jeffrey, Effective application of solid lubricants in spacecraft mechanisms, Lubricants 8 (2020) 74.
[11] M.R. Vazirisereshk, A. Martini, D.A. Strubbe, M.Z. Baykara, Solid lubrication with MoS2: a review, Lubricants 7 (2019) 57.
[12] R. Li, X. Yang, J. Zhao, C. Yue, Y. Wang, J. Li, E. Meyer, J. Zhang, Y. Shi, Operando Formation of van der Waals heterostructures for achieving macroscale superlubricity on engineering rough and worn surfaces, Adv. Funct. Mater. 32 (2022) 1–11.
[13] G. Ru, W. Qi, K. Tang, Y. Wei, T. Xue, Interlayer Friction and Superlubricity in Bilayer Graphene and MoS2/MoSe2 van Der Waals Heterostructures, Tribol. Int. 151 (2020) 106483.
[14] A. Macknojia, A. Ayyagari, D. Zambrano, A. Rosenkranz, E.V. Shevchenko, D. Berman, Macroscale superlubricity induced by MXene/MoS2 nanocomposites on rough steel surfaces under high contact stresses, ACS Nano 17 (2023) 2421–2430.
[15] G. Boidi, D. Zambrano, S. Schwarz, E. Marquis, M. Varga, R. Ripoll, E. Badisch, M. Clelia, C. Gachot, G. Grützmacher, A. Rosenkranz, Solid lubrication performance of hybrid Ti 3 C 2 T x/MoS 2 coatings, Carbon N. Y. 225 (2024) 119067.
[16] M. Naguib, M. Kurtoglu, V. Presser, J. Lu, J. Niu, M. Heon, L. Hultman, Y. Gogotsi, M.W. Barsoum, Two-dimensional nanocrystals produced by exfoliation of Ti3AlC2, Adv. Mater. 23 (2011) 4248–4253.
[17] A.V. Mohammadi, J. Rosen, Y. Gogotsi, The world of two-dimensional carbides and nitrides (MXenes), Science. 372 (2021) 1165.
[18] A. Rosenkranz, M.C. Righi, A.B. Anasori, V. Mochalin, Perspective of 2D MXenes tribology, Adv. Mater. 35 (2023) 2207757.
[19] G. Wang, H. Hou, Y. Yan, R. Jagatramka, A. Shirsalimian, Y. Wang, B. Li, M. Daly, C. Cao, Recent advances in the mechanics of 2D materials, Int. J. Extrem. Manuf. 5 (2023) 032002.
[20] A. Rosenkranz, Y. Liu, L. Yang, L. Chen, 2D nano-materials beyond graphene: from synthesis to tribological studies, Appl. Nanosci. 10 (2020) 3353–3388.
[21] B.C. Wyatt, A. Rosenkranz, B. Anasori, 2D MXenes: tunable mechanical and tribological properties, Adv. Mater. 33 (2021) 2007973.
[22] S. Huang, K.C. Mutyala, A.V. Sumant, V.N. Mochalin, Achieving superlubricity with 2D transition metal carbides (MXenes) and MXene/graphene coatings, Mater. Today Adv. 9 (2021) 100133.
[23] J. Wait, G. Josephson, B.C. Wyatt, B. Anasori, A. Çolak, Environmentally stable nanoscale superlubricity of multi-layered Ti3C2Tx MXene, Carbon N. Y. 213 (2023) 118284.
[24] M. Marian, G.C. Song, B. Wang, V.M. Fuenzalida, S. Krauß, B. Merle, S. Tremmel, S. Wartzack, J. Yu, A. Rosenkranz, Effective usage of 2D MXene nanosheets as solid lubricant – influence of contact pressure and relative humidity, Appl. Surf. Sci. 531 (2020) 147311.
[25] Y. Li, S. Huang, C. Wei, D. Zhou, B. Li, V.N. Mochalin, C. Wu, Friction between MXenes and other two-dimensional materials at the nanoscale, Carbon N. Y. 196 (2022) 774–782.
[26] A. Majed, M. Kothakonda, F. Wang, E.N. Tseng, K. Prenger, X. Zhang, P.O. Å. Persson, J. Wei, J. Sun, M. Naguib, Transition metal carbo-chalcogenide "TMCC: " A new family of 2D materials, Adv. Mater. 34 (2022) 2200574.
[27] O. Beckmann, H. Boller, H. Nowotny, Die Kristallstrukturen von Ta2S2C Und Ti4S5 (Ti0,81S), Monatsh. Chem. 101 (1970) 945–955.
[28] H. Boller, K. Hiebl, Quaternary pseudo-Intercalation phases Tx [Nb2S2C] (TV, Cr, Mn, Fe, Co, Ni, Cu) and Metastable Nb2S2C formed by Topochemical synthesis, J. Alloys Compd. 183 (1992) 438–443.
[29] K. Belay Ibrahim, T. Ahmed Shifa, S. Zorzi, M. Getaye Sendeku, E. Moretti, A. Vomiero, Emerging 2D materials beyond Mxenes and TMDs: transition metal carbo-chalcogenides, Prog. Mater. Sci. 144 (2024) 101287.
[30] P. Wally, M. Ueki, Tribological properties of transition metal carbosulfides and Carbosulfide-metal Composites, Wear 215 (1998) 98–103.
[31] S.M. Aouadi, H. Gao, A. Martini, T.W. Scharf, C. Muratore, Lubricious oxide coatings for Extreme temperature applications: a Review, Surf. Coating. Technol. 257 (2014) 266–277.
[32] T. Maclucas, L. Daut, P. Grützmacher, M.A. Guitar, V. Presser, C. Gachot, S. Suarez, F. Mücklich, Influence of structural depth of laser-Patterned steel surfaces on the solid lubricity of carbon nanoparticle coatings, Friction 11 (2023) 1276–1291.
[33] P.G. Grützmacher, M. Schranz, C.J. Hsu, J. Bernardi, A. Steiger-Thirsfeld, L. Hensgen, M. Rodríguez Ripoll, C. Gachot, Solid lubricity of WS2 and Bi2S3 coatings deposited by plasma spraying and air spraying, Surf. Coating. Technol. 446 (2022) 128772.
[34] A. Rosenkranz, P.G. Grützmacher, R. Espinoza, V.M. Fuenzalida, E. Blanco, N. Escalona, F.J. Gracia, R. Villarroel, L. Guo, R. Kang, F. Mücklich, S. Suarez, Z. Zhang, Multi-layer Ti3C2Tx-nanoparticles (MXenes) as solid lubricants – role of surface terminations and Intercalated water, Appl. Surf. Sci. 494 (2019) 13–21.
[35] D.A. Shirley, High-resolution x-ray Photoemission Spectrum of the valence Bands of Gold, Phys. Rev. B 5 (1972) 4709–4714.
[36] S. Tougaard, Universality Classes of Inelastic electron Scattering cross-Sections, Surf. Interface Anal. 25 (1997) 137–154.
[37] C.D. Wagner, Sensitivity factors for XPS analysis of surface atoms, J. Electron. Spectrosc. Relat. Phenom. 32 (1983) 99–102.
[38] C.D. Wagner, A.V. Naumkin, A. Kraut-Vass, J.W. Allison, C.J. Powell, J.R. Rumble, NIST Standard Reference Database 20, Version 3.4, 2003.
[39] C.D. Wanger, W.M. Riggs, L.E. Davis, J.F. Moulder, G.E. Muilenberg, Handbook of X-Ray Photoelectron Spectroscopy, Perkin-Elmer Corp., Physical Electronics Division, Eden Prairie, Minnesota, USA, 1979.
[40] G. Beamson, D. Briggs, High Resolution XPS of Organic Polymers - the Scienta ESCA300 Database, Wiley, 1992. Appendices 3.1 and 3.2.
[41] P. Giannozzi, S. Baroni, N. Bonini, M. Calandra, R. Car, C. Cavazzoni, D. Ceresoli, G.L. Chiarotti, M. Cococcioni, I. Dabo, A. Dal Corso, S. De Gironcoli, S. Fabris, G. Fratesi, R. Gebauer, U. Gerstmann, C. Gougoussis, A. Kokalj, M. Lazzeri, L. Martin-Samos, N. Marzari, F. Mauri, R. Mazzarello, S. Paolini, A. Pasquarello, L. Paulatto, C. Sbraccia, S. Scandolo, G. Sclauzero, A.P. Seitsonen, A. Smogunov, P. Umari, R.M. Wentzcovitch, Quantum ESPRESSO: a modular and Open-source software project for Quantum simulations of materials, J. Phys. Condens. Matter 21 (2009) 395502.
[42] P. Giannozzi, O. Andreussi, T. Brumme, O. Bunau, M.B. Nardelli, M. Calandra, R. Car, C. Cavazzoni, D. Ceresoli, M. Cococcioni, Others. Advanced capabilities for materials modelling with Quantum ESPRESSO, J. Phys. Condens. Matter 29 (2017) 465901.
[43] P. Giannozzi, O. Baseggio, P. Bonfà, D. Brunato, R. Car, I. Carnimeo, C. Cavazzoni, S. De Gironcoli, P. Delugas, F. Ferrari Ruffino, A. Ferretti, N. Marzari, I. Timrov, A. Urru, S. Baroni, Quantum ESPRESSO toward the exascale, J. Chem. Phys. 152 (2020) 154105.
[44] J.P. Perdew, K. Burke, M. Ernzerhof, Generalized gradient approximation made simple, Phys. Rev. Lett. 77 (1996) 3865–3868.
[45] S. Grimme, Semiempirical GGA-type density functional constructed with a long-range dispersion correction, J. Comput. Chem. 27 (2006) 1787–1799.
[46] E. Marquis, M. Cutini, B. Anasori, A. Rosenkranz, M.C. Righi, Nanoscale MXene interlayer and substrate adhesion for lubrication : a density functional theory study, ACS Appl. Nano Mater. 5 (2022) 10516–10527.
[47] H.J. Monkhorst, J.D. Pack, Special points for brillouin-zone integrations, Phys. Rev. B 13 (1976) 5188.
[48] P.J. Blau, On the nature of running-in, Tribol. Int. 38 (2005) 1007–1012.
[49] H. Terwisscha-Dekker, T. Hogenelst, R. Bliem, B. Weber, D. Bonn, Why Teflon is so slippery while other polymers are not, Phys. Rev. E 107 (2023) 24801.
[50] G. Boidi, D. Zambrano, M.I. Broens, D. Moncada, M. Varga, M.R. Ripoll, E. Badisch, N. Escalona, P.G. Grützmacher, C. Gachot, A. Rosenkranz, Influence of ex-Situ Annealing on the friction and wear performance of Multi-layer Ti3C2Tx coatings, Appl. Mater. Today 36 (2024) 102020.
[51] M. Wolloch, G. Levita, P. Restuccia, M.C. Righi, Interfacial charge density and its connection to adhesion and frictional forces, Phys. Rev. Lett. 121 (2018) 26804.
[52] G. Zilibotti, M.C. Righi, Ab Initio calculation of the adhesion and ideal shear strength of planar Diamond interfaces with different atomic structure and hydrogen coverage, Langmuir 27 (2011) 6862–6867.
[53] M. Wolloch, G. Losi, M. Ferrario, M.C. Righi, High-throughput screening of the static friction and ideal Cleavage strength of solid interfaces, Sci. Rep. 9 (2019) 1–10.
[54] G. Levita, E. Molinari, T. Polcar, M.C. Righi, First-principles comparative study on the interlayer adhesion and shear strength of transition-metal dichalcogenides and graphene, Phys. Rev. B Condens. Matter 92 (2015) 1–8.
[55] M. Seredych, C.E. Shuck, D. Pinto, M. Alhabeb, E. Precetti, G. Deysher, B. Anasori, N. Kurra, Y. Gogotsi, High-temperature behavior and surface chemistry of carbide MXenes studied by thermal analysis, Chem. Mater. 31 (2019) 3324–3332.
[56] P.G. Grützmacher, S. Suarez, A. Tolosa, C. Gachot, G. Song, B. Wang, V. Presser, F. Mücklich, B. Anasori, A. Rosenkranz, Superior wear-resistance of Ti3C2TxMultilayer coatings, ACS Nano 15 (2021) 8216–8224.
[57] A. Rosenkranz, P.G. Grützmacher, R. Espinoza, V.M. Fuenzalida, E. Blanco, N. Escalona, F.J. Gracia, R. Villarroel, L. Guo, R. Kang, F. Mücklich, S. Suarez, Z. Zhang, Multi-layer Ti3C2Tx-nanoparticles (MXenes) as solid lubricants – role of surface terminations and Intercalated water, Appl. Surf. Sci. 494 (2019) 13–21.